



RESEARCH ARTICLE | JANUARY 05 2023


Incomplete activation and ionization of dopants in Si at room temperature

Luigi Abenante  




AIP Advances 13, 015109 (2023)

<https://doi.org/10.1063/5.0117615>



Biomicrofluidics
Special Topic:
Microfluidic Biosensors
Submit Today



Incomplete activation and ionization of dopants in Si at room temperature

Cite as: AIP Advances 13, 015109 (2023); doi: 10.1063/5.0117615

Submitted: 6 August 2022 • Accepted: 6 December 2022 •

Published Online: 5 January 2023



View Online



Export Citation



CrossMark

Luigi Abenante^{a)} 

AFFILIATIONS

ENEA, Italian National Agency for New Technologies, Energy and Sustainable Economic Development, Roma, Italy

^{a)} Author to whom correspondence should be addressed: clovocloodo@gmail.com

ABSTRACT

A new model for incomplete ionization of dopants in Si is presented, where the Fermi level of free carriers may displace with respect to the case of full activation of dopants. The curves of the ratio of free-carrier density and active-dopants density vs doping, which are calculated at partial activation of dopants with the new model, overlap exactly with the curves of the same quantity calculated at full activation of dopants with a reported model. Calculations are performed with and without reported parameterizations of the density of states and occupancy probability of the dopant band simulating incomplete ionization around the Mott concentration. With parameterizations, comparisons with Hall-mobility data show that the curves of free-carrier density calculated at partial dopant activation with the new model are more accurate than the curves of the same quantity calculated at full dopant activation with the reported model. Without parameterizations, the new model allows calculating for the same carrier species curves of majority-carrier mobility that fit measured data of minority-carrier mobility at high dopings and agree with the Klaassen mobility model for minority carriers. The consistency with the band theory of the new and reported models is discussed, and the new model is found to be the most appropriate in this respect. The free-carrier density calculated with the new model without parameterizations overlaps at high dopings with free-carrier density calculated with reported models for band-gap narrowing and allows calculating curves of Auger lifetime of majority carriers that fit measured lifetime data of minority carriers.

© 2023 Author(s). All article content, except where otherwise noted, is licensed under a Creative Commons Attribution (CC BY) license (<http://creativecommons.org/licenses/by/4.0/>). <https://doi.org/10.1063/5.0117615>

I. INTRODUCTION

The conductivity or conductance mobility is

$$\mu_c = \frac{1}{q\rho n}, \quad (1)$$

where ρ is the resistivity, q is the electron charge, and n is the density of conduction or free carriers, which is usually measured in highly doped Si by assuming $n = N$, where N is the measured doping density. Pearson *et al.*¹ first determined in 1950 μ_c in n -type Ge from separate measurements of ρ and n . They assumed that at room temperature, dopants are all ionized, i.e., $n = N$, at $N < 10^{18} \text{ cm}^{-3}$. Haynes and Shockley² used the Pearson *et al.* approach to determine μ_c -values for electrons in n -type Ge to be compared to the measured mobility of electrons injected in p -type Ge, which was called drift mobility, μ_d . In Ref. 2, a good agreement between μ_c and μ_d was found in samples with resistivity ranging from 1.5 to 6 $\Omega\text{-cm}$. The approach of Pearson *et al.*,¹ i.e., separate measurements of ρ and n ,

was followed in the subsequent determinations of majority-carrier mobility. The approach of Haynes and Shockley,² i.e., injection of carriers of a given species in a semiconductor filled with carriers of the opposite species, was followed in the subsequent determinations of minority-carrier mobility. Consequently, μ_c and μ_d can be taken as synonymous of the majority- and minority-carrier mobilities, respectively. Concerning μ_c , despite the Backenstoss suggestion that n can be obtained from N by calculating the fraction of ionized donors or acceptors,³ in the course of the years, assuming $n = N$ also in the high-doping range ($N \geq 10^{18} \text{ cm}^{-3}$) became customary in measuring and modeling μ_c . However, partial ionization of dopants was suggested again for determining μ_c in Refs. 4–9. To a continuous increase with N of such a quantity, as argued in Refs. 4–6, a localized increase around the Mott critical concentration, N_{mott} , was opposed in Refs. 7–9. In Refs. 7 and 8, Altermatt, Schenk, Schmithuesen, and Heiser (ASSH) derived a model for incomplete ionization, where all dopant atoms are “electronically active,”⁷ i.e., $N_a = N$, where N_a is the active-dopant density, at any N -value. To validate their model,

ASSH fit data of μ_c/μ_H , where μ_H is the Hall mobility, in both p - and n -type Si, with n/N -curves calculated by using parameterizations of the density of states and occupancy probability of the dopant band such that, as aforementioned, $n < N$ only occurs in a doping region around the Mott concentration.⁸ In this paper, we propose a new more general model for incomplete ionization, where, in addition to $N_a = N$, assuming $N_a < N$ is also allowed. The phenomenon that will be interpreted differently when using the new formulation compared to Refs. 7 and 8 is, therefore, the activation of dopants. The possibility that $N_a < N$ is considered in the new model by introducing a displacement of the Fermi level with respect to the case of full activation of dopants in the Boltzmann approximations for n . Curves of n/N_a vs N calculated at partial dopant activation with the new model overlap exactly with the curves of n/N vs N calculated with the ASSH model⁸ both with and without the ASSH parameterizations.⁸ Consequently, the $n(N)$ -curves calculated with the new model differ from the $n(N)$ -curves calculated with the ASSH model.⁸ The $n(N)$ -curves obtained with both the new and ASSH models with and without the ASSH parameterizations⁸ are assigned in (1) to calculate $\mu_c(n)$ -curves. With the ASSH parameterizations,⁸ comparisons with μ_H -data extracted from the μ_c/μ_H -data reported in Refs. 7–9 show that around N_{mott} , the n -values calculated with the new model are more accurate than the n -values calculated with the ASSH model.⁸ However, we find that only the new model without the ASSH parameterizations⁸ is consistent with the band theory in the entire high-doping range. In this case, the new model calculates $n \ll N$ already at $N > 10^{18} \text{ cm}^{-3}$ allowing to calculate $\mu_c(n)$ -curves with (1) that fit reported measured $\mu_d(N)$ -data at high dopings and agree closely with $\mu_d(N)$ -curves calculated with the Klaassen mobility model for device simulation.¹⁰ Experimental results have been published (e.g., Refs. 11–19), which show that, in Si at $N > 10^{18} \text{ cm}^{-3}$, for the same carrier species, μ_d exceeds μ_c up to a factor of three at $N = 10^{20} \text{ cm}^{-3}$. To account for such a discrepancy, in the literature, $n = N$ in highly doped Si is “*a priori*” taken for granted, and it is assumed that at $n = N$ minority carriers are less scattered than majority carriers by Coulomb interaction with ionized dopants.²⁰ The results presented in this work allow taking into consideration another possibility, which is that the aforementioned discrepancy may be simply due to the aforementioned conventional assignment $n = N$ in the measurement of μ_c , which may provide underestimated values of this quantity at high dopings. This possibility is corroborated by band-gap narrowing models based on experiments,¹⁸ which calculate curves of majority-carrier density vs N that at high dopings overlap with the $n(N)$ -curves calculated with the new model without parameterizations. As a further confirmation, these $n(N)$ -curves allow calculating curves of Auger lifetime fitting experimental data. As aforementioned, the new model implies that, for the same carrier species, the majority- and minority-carrier mobilities are the same at high dopings. This is contrary to conventional assumptions. The devices and applications that are impacted by the model are consequently Si devices such as JFETs, MOSFETs, and MOS transistors, where currents are calculated by using the majority-carrier mobility,²¹ and the relevant modeling and simulation.

II. MODEL

The ratio of free-carrier density, n , and dopant density, N , can be expressed by using the Fermi–Dirac statistics as²¹

$$\frac{n}{N} = 1 - \frac{1}{1 + g \exp[(E_D - E_F)/kT]} \quad (2)$$

in n -type Si, and²¹

$$\frac{n}{N} = 1 - \frac{1}{1 + g \exp[-(E_D - E_F)/kT]} \quad (3)$$

in p -type Si, where g is the degeneracy factor, E_F is the Fermi energy, E_D is the dopant energy, k is the Boltzmann constant, and T is the absolute temperature. It is worth mentioning that (2) and (3) are derived by assuming $N = n + N_0$, where N_0 is the density of bound carriers, and the ratio at the right members of (2) and (3) represents the occupation probability of the dopant level, $f(E_D)$. As long as the Fermi–Dirac distribution can be approximated by the Boltzmann distribution, n can be calculated with the widely used Boltzmann expressions as

$$n = N_C \exp[-(E_C - E_F)/kT] \quad (4)$$

in n -type Si, and

$$n = N_V \exp[(E_V - E_F)/kT] \quad (5)$$

in p -type Si,^{21,22} where E_C is the energy at the bottom of the conduction band, E_V is the energy at the top of the valence band, N_C is the effective density of states in the conduction band, and N_V is the effective density of states in the valence band. Due to the aforementioned assumption that $n = N$ at room temperature,²¹ (4) and (5) are required to converge to

$$N = N_C \exp[-(E_C - E_F)/kT] \quad (6)$$

and

$$N = N_V \exp[(E_V - E_F)/kT], \quad (7)$$

respectively, at room temperature.²¹ Altermatt, Schenk, Schmithuesen, and Heiser (ASSH) neglect the possibility that not all dopant atoms are “electronically active,”²⁷ i.e., $N_a < N$, where N_a is the active-dopant density. We take into account such a possibility by exploiting the fact that the Fermi-energy level is sensitive to charge-density variations. We model (6) and (7) as

$$N = N_C \exp\{-[E_C - (E_{F0} - \Delta E_F)]/kT\} \quad (8)$$

and

$$N = N_V \exp\{[E_V - (E_{F0} - \Delta E_F)]/kT\}, \quad (9)$$

respectively, with E_{F0} being a Fermi level defined as $E_{F0} = E_F + \Delta E_F$, where ΔE_F is an energy displacement, so that by using (8) and (9), N_a can be defined as

$$N \exp(\Delta E_F/kT) = N_a = N_C \exp[-(E_C - E_{F0})/kT] \quad (10)$$

in *n*-type Si, and

$$N \exp(-\Delta E_F/kT) = N_a = N_V \exp[(E_V - E_{F0})/kT] \quad (11)$$

in *p*-type Si, and, hence, be equal to *N* when $\Delta E_F = 0$ eV. In such a way, (10) and (11) model the general case, where both $N_a = N$ and $N_a < N$ are allowed at any *N*-value, which reduces to (6) and (7) in the particular case, where $N_a = N$. Assigning $E_F = E_{F0}$ as calculated with (10) and (11) in (2) and (3), respectively, and assuming $N_a = n + N_0$ allows expressing the ratio of free-carrier density and active-dopant density as

$$\frac{n}{N_a} = 1 - \frac{N_a}{N_a + gN_C \exp[(E_D - E_C)/kT]} \quad (12)$$

and

$$\frac{n}{N_a} = 1 - \frac{N_a}{N_a + gN_V \exp[(E_V - E_D)/kT]} \quad (13)$$

in *n*-type Si and *p*-type Si, respectively.

III. VALIDATION

Altermatt, Schenk, Schmithuesen, and Heiser (ASSH) express n/N as⁸

$$\frac{n}{N} = 1 - \frac{bn}{n + gN_C \exp(-E_D/kT)} \quad (14)$$

in *n*-type Si and

$$\frac{n}{N} = 1 - \frac{bn}{n + gN_V \exp(-E_D/kT)} \quad (15)$$

in *p*-type Si, by parameterizing $f(E_D)$ and E_D such as $n/N < 1$ around N_{mott} . In particular, ASSH multiply $f(E_D)$ by $b = [1 + (N/N_b)^d]^{-1}$, where N_b and d are adjustable parameters,⁸ and parameterize E_D as $E_D = E_{D0}/[1 + (N/N_{ref})^c]$, where E_{D0} is the constant energy level of dopants in Si and N_{ref} and c are adjustable parameters.⁸ Iterating (14) in *n*-type Si and (15) in *p*-type Si with the assignments to N_b , d , N_{ref} , and c for P:Si and B:Si, respectively, which are reported in Ref. 8, at the same E_{D0} - and g -values as used in Ref. 8 and N_C and N_V being given the 300°K values from Ref. 23 yields the curves of n/N that are drawn with full lines in Fig. 1, where measured n/N -curves from Ref. 24 are also reported. The aforementioned ASSH parameterizations⁸ can be removed from (14) and (15) by assigning $E_D = E_{D0}$ and $b = 1$ while leaving the assignments to g , N_C , and N_V unchanged. Iterating (14) and (15) without parameterizations yields the curves of n/N that are drawn with dashed lines in Fig. 1. In the model presented in this work, N_a , n , and ΔE_F can be calculated with and without the ASSH parameterizations⁸ by solving iteratively the equation system

$$\begin{cases} N_a = N \exp\left(\frac{\Delta E_F}{kT}\right), & a \\ \frac{n}{N_a} = 1 - \frac{bN_a}{N_a + gN_C \exp[(E_D - E_C)/kT]}, & b \\ \Delta E_F = kT \ln\left(\frac{n}{N_a}\right) & c \end{cases} \quad (16)$$

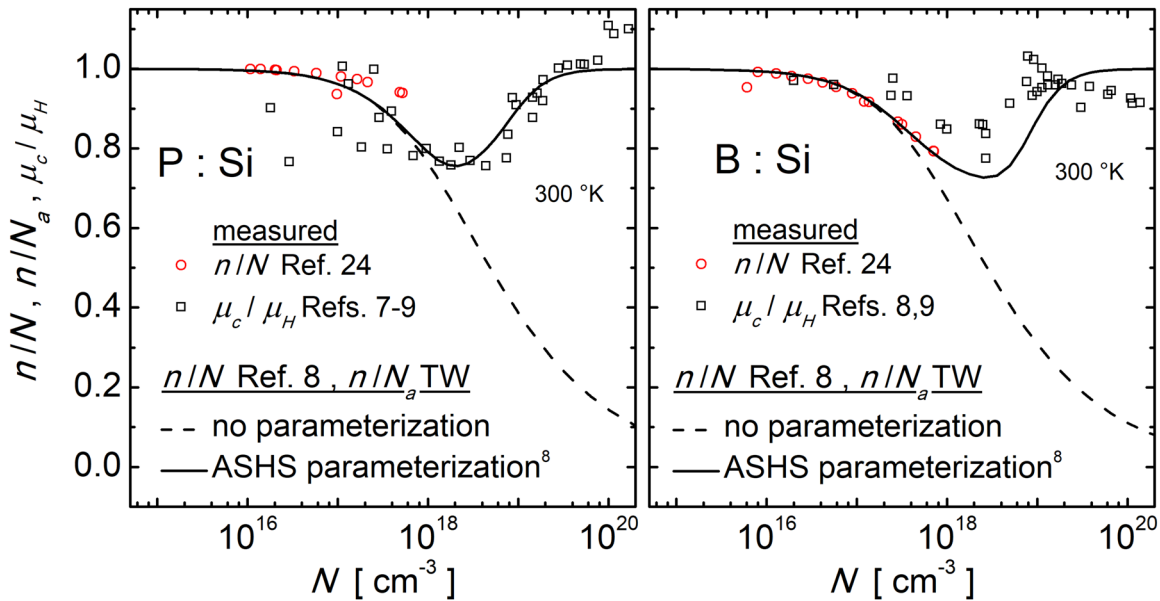


FIG. 1. n/N -curves calculated in Ref. 8 with (14) and (15) and n/N_a -curves calculated in this work with (12) and (13) without (dashed lines) and with (full lines) ASSH parameterizations.⁸ Reported values of μ_c/μ_H and n/N are shown.

in *n*-type Si, and the equation system

$$\begin{cases} N_a = N \exp\left(-\frac{\Delta E_F}{kT}\right), & \text{a} \\ \frac{n}{N_a} = 1 - \frac{bN_a}{N_a + gN_V \exp[(E_V - E_D)/kT]}, & \text{b} \\ \Delta E_F = -kT \ln\left(\frac{n}{N_a}\right) & \text{c} \end{cases} \quad (17)$$

in *p*-type Si. In solving (16), attention must be paid to the fact that E_D cannot be higher than E_C ,^{25,26} and hence, $-E_{D0}$ must be assigned. This can be neglected in the ASSH model, where $-E_D$ is directly assigned in *n*-type Si,⁸ as can be seen in (14). At each N -value, iterations end when

$$\frac{n}{N_a} \approx \frac{N_a}{N}. \quad (18)$$

Both with and without the parameterizations of ASSH⁸ iterating (16) in *n*-type Si and (17) in *p*-type Si yield n/N_a -curves that reproduce exactly the n/N -curves obtained with (14) in *n*-type Si and (15) in *p*-type Si, respectively. This is due to (18) and the fact that, both with and without the ASSH parameterizations,⁸ n as calculated with (14) in *n*-type Si and (15) in *p*-type Si is equal to N_a as calculated with (12) in *n*-type Si and (13) in *p*-type Si, respectively, as can be seen in Fig. 2. Consequently, n as calculated in this work and n as calculated in Ref. 8 do not have necessarily the same value, as can be seen in Fig. 2 as well. Figure 2 shows in addition that the

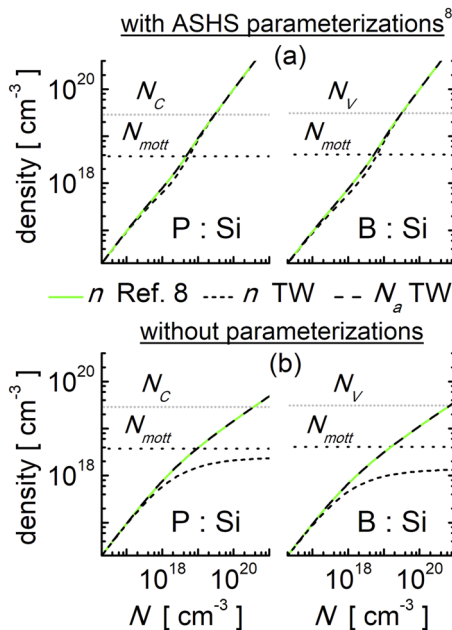


FIG. 2. Curves of $n(N)$ calculated with the model used in Ref. 8 (green lines) and curves of $n(N)$ and $N_a(N)$ calculated with the model presented in this work (TW) (black lines) with and without the ASSH parameterizations.⁸ The N_C , N_V , and N_{mott} -values used by ASSH⁸ are reported.

discrepancy between the model presented in this work and the ASSH model⁸ is more remarkable without parameterizations.

IV. COMPARISONS

ASSH assume⁸

$$\frac{\mu_c}{\mu_H} = \frac{n}{N} \quad (19)$$

and validate the calculated n/N -curves by comparisons with data of μ_c/μ_H ,⁸ as shown in Fig. 1. The μ_c/μ_H -data were obtained by measuring μ_H and μ_c in the same samples.⁷ Moreover, incomplete ionization is neglected in μ_c but included in μ_H .⁷ Consequently, the μ_H -data can be extracted from the μ_c/μ_H -data using

$$\mu_H = \frac{\mu_c(N)}{[\mu_c/\mu_H]}, \quad (20)$$

and (19) implies that

$$\mu_H = \mu_c(N) \frac{N}{n}. \quad (21)$$

We calculate $\mu_c(N)$ in (20) and (21) with (1) at $n = N$ and $\rho(N)$ being calculated with the expressions in Refs. 27 and 28. In (20), the N -values of the samples, where the μ_c/μ_H -data are measured, are used. The μ_H data and curves calculated with (20) and

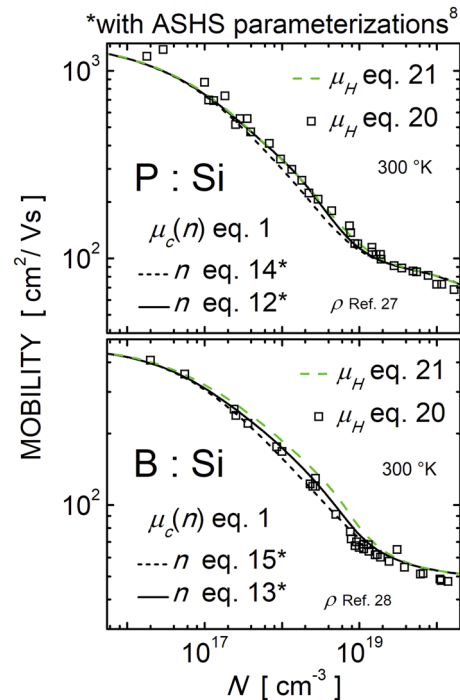


FIG. 3. Curves of mobility vs N calculated with (1) using different assignments to n (black lines) are compared to μ_H -values extracted with (20) from the μ_c/μ_H -values shown in Fig. 1 (hollow squares) and μ_H -curves calculated with (21) (green dashed lines).

(21), respectively, are compared in Fig. 3 to $\mu_c(n)$ -curves calculated with (1) using the $n(N)$ -curves relevant to the ASSH parameterizations,⁸ which are shown in Fig. 2(a), and $\rho(n)$ -curves calculated with the expressions in Refs. 27 and 28. As can be seen, around N_{mott} , the $n(N)$ -curves calculated with the model presented in this work appear to be more accurate than the $n(N)$ -curves calculated with the model presented in Ref. 8. Regarding these comparisons, it should be noted that (20) and (21) agree with each other as long as n/N -curves agree with the μ_c/μ_H -data. As can be seen in Fig. 1, this only occurs in n -type Si. Regarding μ_H , it is worth mentioning that, rather than a conduction mobility, it seems to be a drift mobility.²⁹

We repeat the calculation of $\mu_c(n)$ by assigning in (1) the n -curves calculated without any parameterization, which are shown in Fig. 2(b). The obtained $\mu_c(n)$ -curves are drawn in Fig. 4, where they are compared to reported measurements of μ_d (symbols), $\mu_d(N)$ -curves calculated with the Klaassen mobility model for device simulation¹⁰ in the simulation program PC1D6³⁰ (gray full lines), and curves of the mobility contribution from electron-hole scattering, $\mu_{eh}(N)$, which are calculated according to Klaassen¹⁰ (dotted lines). As can be seen, the $n(N)$ -curves calculated with the model

presented in this work yield $\mu_c(n)$ -curves of majority electrons and holes that fit $\mu_d(N)$ -data of minority electrons and holes, respectively, and agree with the $\mu_d(N)$ -curves calculated with the Klaassen mobility model¹⁰ at all dopings. The $n(N)$ -curves calculated with the model presented in Ref. 8 yield, instead, $\mu_c(n)$ -curves for electrons and holes that only agree with $\mu_d(N)$ -curves and data at medium-low dopings, where they cannot be distinguished from majority-carrier mobility.

V. DISCUSSION

ASSH⁸ obtain (14) and (15) by substituting (4) in

$$\frac{n}{N} = 1 - \frac{b}{1 + g \exp[-(E_F + E_D - E_C)/kT]} \quad (22)$$

in n -type Si, and (5) in

$$\frac{n}{N} = 1 - \frac{b}{1 + g \exp[-(E_D - E_F + E_V)/kT]} \quad (23)$$

in p -type Si, at all dopings. Boltzmann approximations for n are substituted in (22) and (23) in Refs. 25 and 26 as well, to calculate the n/N -curves. Moreover, in Refs. 25 and 26, the $E_d(N)$ -curves are used, which, in Fig. 5, are compared to the $E_d(N)$ -curves used by ASSH.⁸ The modeling approach in Refs. 25 and 26 is then similar to the modeling approach in Ref. 8. However, in Refs. 25 and 26, the n/N -values are not calculated at high dopings.

According to the band theory, n can be assigned (4) and (5) only if the occupation probabilities of E_C and E_V , $f(E_C)$ and $f(E_V)$, respectively, are such as²¹

$$f(E_C) = \frac{1}{1 + \exp[(E_C - E_F)/kT]} \approx \exp[-(E_C - E_F)/kT] \quad (24)$$

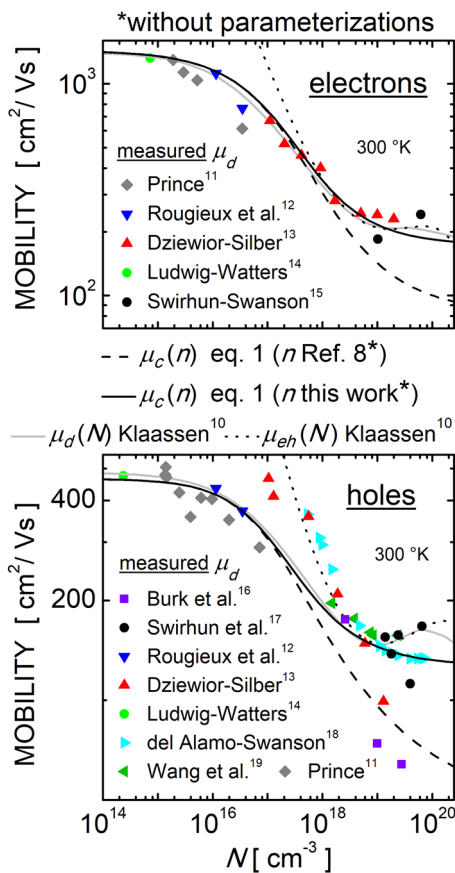


FIG. 4. Curves of conductance mobility vs N calculated with (1) using various assignments to n are compared to measured $\mu_d(N)$ -values^{11–19} (symbols) and mobility curves calculated after Ref. 10.

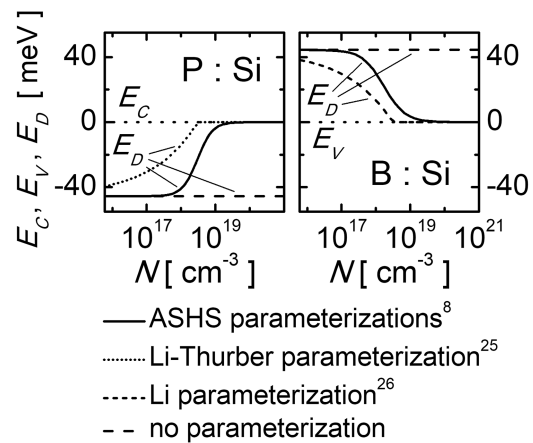


FIG. 5. $E_D(N)$ calculated according to reported parameterizations and without parameterizations.

in *n*-type Si, and

$$f(E_V) = \frac{1}{1 + \exp[-(E_V - E_F)/kT]} \approx \exp[(E_V - E_F)/kT] \quad (25)$$

in *p*-type Si. In Fig. 6, $E_F(N)$ -curves calculated with (4) and (5) using the $n(N)$ -curves reported in Fig. 2 are shown along with $E_F(N)$ -curves calculated with (4) and (5) at $n = N$. In the same figure, $\Delta E_F(N)$ -curves calculated with (16) and (17) are also reported. As can be seen, only the $E_F(N)$ -curves calculated with the model presented in this work without the ASSH parameterizations⁸ are capable of satisfying (24) and (25) in the whole high-doping range, making the Boltzmann statistics a reasonable approximation for Fermi-Dirac. Consequently, only the full-line $\mu_c(n)$ -curves, which, in Fig. 4, fit μ_d -data, are in perfect agreement with the band theory at high dopings. As aforementioned, experimental results show that, in Si at $N > 10^{18} \text{ cm}^{-3}$, for the same carrier species, μ_d exceeds μ_c up to a factor of three at $N = 10^{20} \text{ cm}^{-3}$. Based on the results obtained in this work, such a discrepancy may be ascribed to the conventional assumption of full dopant ionization at all dopings in measuring μ_c , which may involve underestimating the experimental values of this quantity at high dopings. On the other hand, the $E_F(N)$ -curves calculated with (4) and (5) at $n = N$ that are drawn in Fig. 6 with short-dotted lines are inconsistent with (22) and (23) at high dopings

and, hence, do not allow deriving any of the models studied in this work in that doping range.

Klaassen models μ_c as follows:¹⁰

$$\frac{1}{\mu_{ionD}(N)} = \frac{1}{\mu_c(N)} - \frac{1}{\mu_L}, \quad (26)$$

where μ_{ionD} is the mobility due to ionized dopants, μ_L is the lattice scattering mobility, and μ_c is assigned the empirical expression of Masetti *et al.*³¹ Based on (26), μ_{ionD} is homogeneous with μ_c and, hence, is a species of conductivity mobility. In Fig. 4, the Klaassen $\mu_d(N)$ -curves¹⁰ and the Klaassen $\mu_{eh}(N)$ -curves¹⁰ overlap with each other at high dopings. This is consistent with the theory that injected carriers are mostly subjected to the carrier-carrier scattering at high dopings.³² However, in the Klaassen mobility model, $\mu_{eh}(N)$ is modeled as a fraction of $\mu_{ionD}(N)$ and, hence, can be considered as a conductive mobility. $\mu_c = \mu_d$ at high dopings then appears to be consistent with the Klaassen mobility model as well. On the other hand, as aforementioned, μ_H can be considered as a drift mobility. This results from the standard definition of the Hall correction factor,^{29,33}

$$r = \frac{\mu_H}{\mu_d}. \quad (27)$$

ASSH, instead, use^{7,9}

$$r = \frac{\mu_H}{\mu_c}. \quad (28)$$

VI. APPLICATIONS

A change with N of the electron-hole product at thermal equilibrium with respect to its value in undoped Si, n_i^2 , is observed in highly doped Si.^{18,34,35} This change is due to the anomalous increase of minority-carriers density compared to the expected value n_i^2/N . To model the increase of minority carriers, an “apparent” energy band-gap narrowing (BGN), ΔE_g , was introduced,^{18,34,35} such that an “effective” doping density, N_e , can be calculated as

$$N_e = N \exp(-\Delta E_g/kT), \quad (29)$$

and the enhanced minority-carriers density at high dopings can be assigned n_i^2/N_e . Therefore, N_e represents the “effective” density of free majority carriers. N_e and ΔE_g have been denoted as “effective” and “apparent,” respectively, because, although sufficient for device modeling, they are retained to have a doubtful physical significance.¹⁸ Many empirical expressions for ΔE_g have been proposed (see Refs. 18, 34, and 35). In Fig. 7, $N_e(N)$ -curves obtained with five BGN models^{18,35} are compared to the $n(N)$ -curves (full lines) calculated in the present work with (16) and (17) without the ASSH parameterizations,⁸ which are shown in Fig. 2(b) as well. As can be seen in Fig. 7, there is remarkable agreement at high dopings between the $n(N)$ -curves and some of the $N_e(N)$ -curves. On the other hand, an analogy between (29) and (16 a) or (17 a) is undeniable as well as the fact that a change in the bandgap E_g involves a change in E_F . These observations along with the results shown in Fig. 7 allow providing a physical meaning to N_e and ΔE_g .

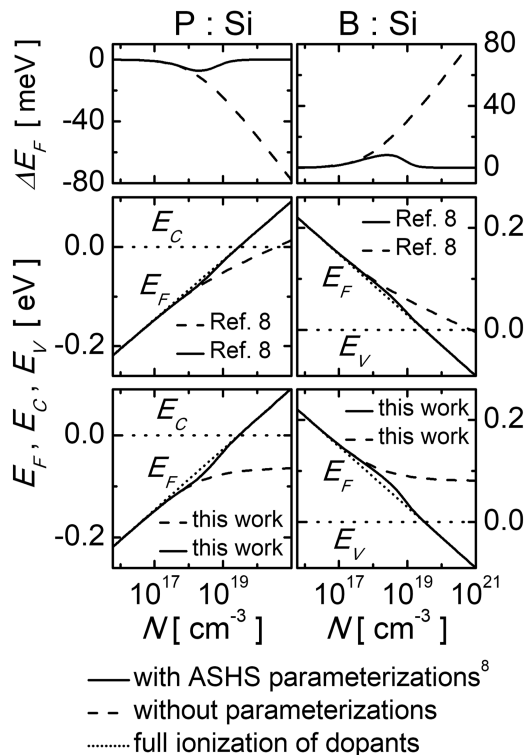


FIG. 6. $E_F(N)$ -curves calculated with (4) and (5) using the $n(N)$ -curves shown in Fig. 2. $E_F(N)$ -curves calculated with (4) and (5) at $n = N$ and $\Delta E_F(N)$ -curves calculated with (16) and (17) are also shown.

As aforementioned, ΔE_g is empirically determined.^{18,34,35} Figure 7 shows that ΔE_g is adjusted such that $N_e \rightarrow n$ at high dopings. N_e and ΔE_g appear then to be equivalent to N_a and ΔE_F under the condition that ΔE_F is such that $N_a = n$ at high dopings. The $N_e(N)$ -curves shown in Fig. 7 are consequently deformations of the $N_a(N)$ -curves shown in Fig. 2. At any rate, all the BGN models are fits to measured data. Consequently, the comparisons in Fig. 7 corroborate experimentally the physical validity of the $n(N)$ -curves calculated with (16) and (17) without parameterizations in the present work, which yield the full-line $\mu_c(n)$ -curves, which, in Fig. 4, fit μ_d -data,

Hangleiter and Haecker introduced an enhancement of minority-carrier Auger recombination due to Coulomb interactions among carriers³⁶ to express the Auger lifetime, τ_A , at any N -value as

$$\tau_A = \frac{\tau_{HD}}{g_{enh}}, \quad (30)$$

where g_{enh} is an Auger-recombination enhancement factor and

$$\tau_{HD} = \frac{1}{C_{HD}N^2} \quad (31)$$

is the lifetime in the high-doping range (10^{19} – 10^{20} cm⁻³) with C_{HD} -values depending on the doping species. The Hangleiter and Haecker approach was adopted in subsequent Auger lifetime models (e.g., Refs. 32, 37, and 38). In these models, g_{enh} has the form

$$g_{enh} = g_{0,enh} + f(n), \quad (32)$$

where $g_{0,enh} = 1$ and $f(n)$ is a function such that $g_{enh} \rightarrow 1$ in the high-doping range. In Fig. 8, $\tau_A(N)$ - and $g_{enh}(n)$ -curves for minority holes and electrons are reported (short-dashed lines) as calculated in P:Si and B:Si, respectively, with (30) and (32) using the relevant Altermatt *et al.*³² parameterizations of C_{HD} and $f(n)$ at $n = N$ as in Ref. 32. Using the parameterizations in Ref. 38 gives less accurate results at low dopings. The parameterizations in Ref. 37 have not

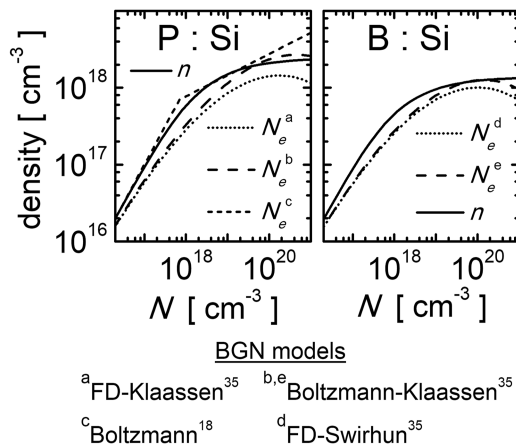


FIG. 7. Comparisons between the majority-carrier density, N_e , implied by five BGN models reported in the literature and the $n(N)$ -curves calculated with (16) and (17) without parameterizations in the present work, which are also shown in Fig. 2(b).

been checked. As can be seen, $\tau_A(N)$ -curves reduce to the Dzierwior and Schmid³⁹ lifetime, τ_{DS} , at high dopings. We calculate $\tau_A(N)$ -curves for the majority holes and electrons in B:Si and P:Si, respectively, with (30) by assigning in (32) the relevant $n(N)$ -curves calculated in the present work with (16) and (17) without the ASHS parameterizations,⁸ which are shown in Figs. 2(b) and 7. In (32), $g_{0,enh} = 0.80544$ and $g_{0,enh} = 0.802208$ are assigned in B:Si and P:Si, respectively, to impose $g_{enh} = 1$ at high dopings, and the Altermatt *et al.* assignments for minority carriers³² are assigned to majority carriers. For example, the parameterization of $f(N)$ for minority electrons in B:Si³² is used for majority electrons in P:Si. The resulting $g_{enh}(n)$ - and $\tau_A(n)$ -curves for majority carriers (full-line curves) are compared in Fig. 8 to the corresponding $g_{enh}(N)$ - and $\tau_A(N)$ -curves for minority carriers (short-dashed line curves). As can be seen, all the τ_A -curves fit lifetime data (symbols), which are taken from Refs. 16, 18, 38–43. This means that, as well as measured mobility, measured lifetime is the same for minority and majority carriers of the same species. The comparisons in Fig. 8 further confirm experimentally the physical validity of the $n(N)$ -curves calculated with (16) and (17) without parameterizations, which yield the full-line $\mu_c(n)$ -curves, which, in Fig. 4, fit μ_d -data. It is worth mentioning that evaluations of majority-carrier lifetime have not been reported so far in the literature.

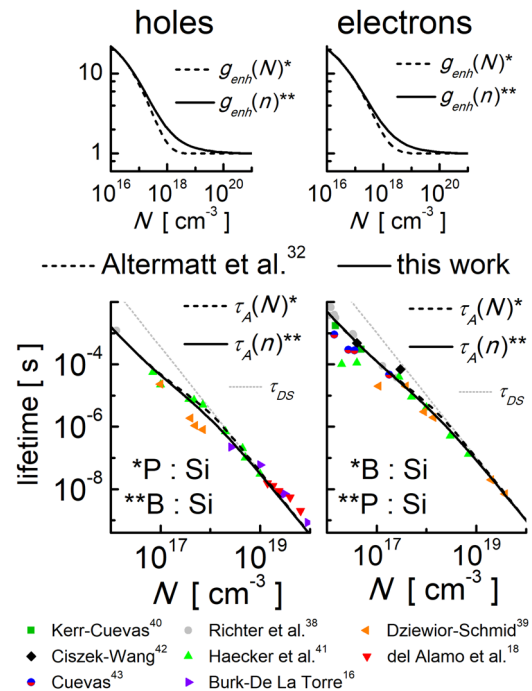


FIG. 8. Comparisons among experimental values of the hole and electron lifetime in doped Si (symbols), $\tau_A(N)$ -curves calculated with (30) using the shown $g_{enh}(N)$ -curves³² (short-dashed line), and $\tau_A(n)$ -curves calculated with (30) using the shown $g_{enh}(n)$ -curves (full line). The $g_{enh}(n)$ -curves are calculated with the $n(N)$ -curves obtained with (16) and (17) without parameterizations, which are shown in Figs. 2(b) and 7. $\tau_A(N)$ is the lifetime of the minority carriers. $\tau_A(n)$ is the lifetime of the majority carriers.

02 May 2024 09:28:50

VII. CONCLUSION

In this work, a reported model for incomplete ionization of dopants in Si has been modified to include the possibility that not all the dopants are active at room temperature. The most important achievement of the new model is the exact calculation of curves of free-carrier density vs doping that are most coherent as possible with the conventional band theory using Fermi–Dirac statistics and Boltzmann statistics. These curves are such that, at room temperature, free-carrier density is much lower than dopant density at medium–high dopings. This is inconsistent with both the common assumption of full dopant ionization at all doping levels at room temperature and the aforementioned reported model for incomplete ionization, which only forecasts partial ionization around the Mott concentration. The new model is, instead, consistent with both reported experimental models for bandgap narrowing and lifetime data. An important consequence of the model presented in this work is that using the aforementioned new curves of free-carrier density to calculate conductance mobility leads to a new interpretation of this quantity in Si. In particular, we find that, contrary to the conventional assumption, for the same carrier species, the majority- and minority-carrier mobilities are the same not only at low dopings but also at high dopings. This implies that available measurements of conductance mobility are affected by a systematic error due to the aforementioned conventional postulation that at room temperature all dopant atoms are ionized not only at low dopings but also at high dopings. Since, in most electron devices such as JFETs, MOSFETs, and MOS transistors, currents are calculated using the majority-carrier mobility, the results presented in this work could be of interest to device designers and Technology CAD/modeling experts concerned with Si.

AUTHOR DECLARATIONS

Conflict of Interest

The author has no conflicts to disclose.

Author Contributions

Luigi Abenante: Conceptualization (equal).

DATA AVAILABILITY

The data that support the findings of this study are available from the corresponding author upon reasonable request.

REFERENCES

- G. L. Pearson, J. D. Struthers, and H. C. Theuerer, *Phys. Rev.* **77**, 809 (1950).
- J. R. Haynes and W. Shockley, *Phys. Rev.* **81**, 835 (1951).
- G. Backenstoss, *Phys. Rev.* **108**, 1416 (1957).
- H. Watanabe and S.-i. Takagi, *J. Appl. Phys.* **90**, 1600 (2001).
- G. Xiao, J. Lee, J. J. Liou, and A. Ortiz-Conde, *Microelectron. Reliab.* **39**, 1299 (1999).
- Y. Yue and J. J. Liou, *Solid-State Electron.* **39**, 318 (1996).
- P. P. Altermatt, A. Schenk, and G. Heiser, *J. Appl. Phys.* **100**, 113714 (2006).
- P. P. Altermatt, A. Schenk, B. Schmithüsen, and G. Heiser, *J. Appl. Phys.* **100**, 113715 (2006).
- A. Schenk, P. P. Altermatt, and B. Schmithuesen, International Conference on Simulation of Semiconductor Processes and Devices, Monterey, CA, 2006, pp. 51–54.
- D. B. M. Klaassen, *Solid-State Electron.* **35**, 953–959 (1992).
- M. B. Prince, *Phys. Rev.* **93**, 1204 (1954).
- F. E. Rougieux, D. Macdonald, A. Cuevas, S. Ruffell, J. Schmidt, B. Lim, and A. P. Knights, *J. Appl. Phys.* **108**, 013706 (2010).
- J. Dziejwior and D. Silber, *Appl. Phys. Lett.* **35**, 170–172 (1979).
- G. W. Ludwig and R. L. Watters, *Phys. Rev.* **101**, 1699 (1956).
- S. E. Swirhun and R. M. Swanson, Technical Report NASA-CR-180608, JPL-9950-1256, DOE/JPL-957159-86/2, NAS 1.26:180608, 1986.
- D. E. Burk and V. de la Torre, *IEEE Electron Device Lett.* **5**, 231 (1984).
- S. E. Swirhun, J. A. del Alamo, and R. M. Swanson, *IEEE Electron Dev. Lett.* **7**, 168–171 (1986).
- J. A. del Alamo and R. M. Swanson, *IEEE Trans. Electron Dev.* **34**, 1580 (1987).
- C. H. Wang, K. Misiakos, and A. Neugroschel, *IEEE Trans. Electron Dev.* **37**, 1314 (1990).
- H. S. Bennett, *Solid-State Electron.* **28**, 193–200 (1985).
- J. P. Colinge and C. A. Colinge, *Physics of Semiconductor Devices* (Kluwer Academic Publishers, New York, Boston, Dordrecht, London, Moscow, 2005).
- M. A. Green, *Solar Cells: Operating Principles, Technology, and System Applications* (Prentice-Hall, Englewood Cliffs, NJ, 1982).
- M. A. Green, *J. Appl. Phys.* **67**, 2944 (1990).
- W. R. Thurber, R. L. Mattis, Y. M. Liu, and J. J. Filliben, *The Relationship between Resistivity and Dopant Density for Phosphorus- and Boron-Doped Silicon* (NBS Special Publication, 1981), pp. 400–464.
- S. S. Li and W. R. Thurber, *Solid-State Electron.* **20**, 609–616 (1977).
- S. S. Li, *Solid-State Electron.* **21**, 1109–1117 (1978).
- W. R. Thurber, R. L. Mattis, Y. M. Liu, and J. J. Filliben, *J. Electrochem. Soc.* **127**, 1807–1812 (1980).
- W. R. Thurber, R. L. Mattis, Y. M. Liu, and J. J. Filliben, *J. Electrochem. Soc.* **127**, 2291–2294 (1980).
- H. Nakagawa and S. Zukotynski, *Can. J. Phys.* **56**, 364 (1978).
- H. Haug and J. Greulich, *Energy Procedia* **92**, 60–68 (2016).
- G. Masetti, M. Severi, and S. Solmi, *IEEE Trans. Electron Dev.* **30**, 764 (1983).
- P. P. Altermatt, J. Schmidt, G. Heiser, and A. G. Aberle, *J. Appl. Phys.* **82**, 4938 (1997).
- Subcommittee F01.15 on Compound Semiconductors, ASTM F76-08(2016)e1, “Standard test methods for measuring resistivity and hall coefficient and determining hall mobility in single-crystal semiconductors,” ASTM International, 2016.
- D. Yan and A. Cuevas, *J. Appl. Phys.* **114**, 044508 (2013).
- D. Yan and A. Cuevas, *J. Appl. Phys.* **116**, 194505 (2014).
- A. Hangleiter and R. Häcker, *Phys. Rev. Lett.* **65**, 215 (1990).
- J. Schmidt, M. Kerr, and P. P. Altermatt, *J. Appl. Phys.* **88**, 1494 (2000).
- A. Richter, S. W. Glunz, F. Werner, J. Schmidt, and A. Cuevas, *Phys. Rev. B* **86**, 165202 (2012).
- J. Dziejwior and W. Schmidt, *Appl. Phys. Lett.* **31**, 346–348 (1977).
- M. J. Kerr and A. Cuevas, *Semicond. Sci. Technol.* **17**, 35 (2002).
- R. Haecker and A. Hangleiter, *J. Appl. Phys.* **75**, 7570 (1994).
- T. F. Cizek and T. H. Wang, in *Proceedings of the 14th European Photovoltaic Solar Energy Conference, Barcelona, Spain* (H Stephens and Associates, Bedford, UK, 1997), p. 103.
- A. Cuevas, *Sol. Energy Mater. Sol. Cells* **57**, 277–290 (1999).